Analysis of mechanical properties and microstructure of high-silicon dual-phase steel

H. K. D. H. Bhadeshia and D. V. Edmonds

The application of available two-phase deformation models to dual-phase steels is examined by testing them against available data published in the literature and an experimental high-silicon-containing steel. It is shown that the successful prediction of mechanical properties by the models depends critically on the strain distribution between the two phases of the steels examined. A detailed characterization by transmission electron microscopy of the hard phases obtained in the high-silicon steel is also carried out. Hard-phase structures consisting either of platelet martensite or of carbide-free upper bainite were identified, and both of these structures contained significant amounts of retained austenite.

Manuscript received 25 April 1979; in final form 15 August 1979.
H. K. D. H. Bhadeshia, BSc, is and D. V. Edmonds, MA, BSc, PhD, was in the Department of Metallurgy and Materials Science, University of Cambridge. Dr Edmonds is now in the Department of Metallurgy and Science of Materials, University of Oxford.

The term dual-phase steels has been used to describe the product of recent process/structure modifications to conventional HSLA steels. They can most conveniently be defined as low-carbon low-alloy ferritic steels with an aggregate microstructure of ferrite and a non-pearlitic hard phase (e.g. martensite). Their potential as superior strength and formability substitutes for current automotive steels in the USA was recognized at an early stage[1, 2] and has provided an incentive for their rapid development and acceptance in this role. This successful application has preceded the acquisition of a complete understanding of the detailed relationships between their process route, microstructure, and mechanical properties, although some research has been carried out in order to optimize the variables in the strength/formability balance.

Steel composition has been one of the aspects studied, and it appears that the use of high silicon additions ($\sim$2 wt-%) results in better combinations of strength and formability.[3–6] Silicon in solid solution not only increases strength but its presence also raises the tensile stress to yield stress ratio and at the same time eliminates discontinuous yielding.[3] This last is important in the avoidance of stretcher strain markings during forming operations. Considering its ability to increase strength by its presence in solid solution, silicon has a minimal detrimental effect on ductility.[4] Silicon is also known to retard martensite tempering reactions[7–9] and often eliminates autotempering altogether.[10] This effect should increase the strength of the martensitic component of dual-phase structures since carbon will then remain in interstitial solid solution in the martensite lattice.

The hardenability of dual-phase steels is generally critically balanced in order to achieve the necessary microstructure using continuous production processes, while at the same time being compatible with the weldability, strength, and ductility requirements. However, little attention has been paid to the detailed microstructure of the hard phase, which is in turn a function of the hardenability of the residual austenite. In the case of high-silicon heat-treatable steels, it has been shown that the best strength and toughness combination is achieved with a homogeneous upper-bainitic microstructure.[11] It should be noted that upper bainite in high-silicon steels consists of alternating layers of high-carbon retained austenite and interstitial-free dislocated bainitic ferrite.[10, 12] Furthermore, the properties of high-silicon steels are extremely structure sensitive.[11] In the present study the microstructure and mechanical properties of an experimental high-silicon dual-phase steel are examined in detail.

The most important property characteristic of dual-phase steels, at least so far as their application in cold-pressing operations is concerned, is their high strain hardening coefficient. A high strain hardening coefficient, or n value, stabilizes tensile deformation against local instability and results in a greater degree of uniform elongation. In order to test the experimental behaviour of dual-phase steels, and eventually to achieve a predictive capability for structure–property relationships, a working model of the deformation of a composite consisting of two ductile components is required. Before the experimental results of the present work are considered, an evaluation is made of two available deformation models with respect to their useful application to dual-phase steels.

DEFORMATION MODELS FOR DUAL-PHASE STEELS

One model successfully used[13, 14] to obtain the deformation parameters of dual-phase steels is that of Mileiko.[15] The use of Mileiko's theory has been stimulated by its ability to predict directly the strain hardening coefficient (the latter being equivalent to the true uniform elongation of a ductile phase) of the composite concerned. The relationship between the volume fraction V of the second phase and the mechanical properties of the composite and of the component phases is given by

$$V = \frac{1}{1+\beta\dfrac{\varepsilon_c-\varepsilon_m}{\varepsilon_f-\varepsilon_c}\varepsilon_c^{\varepsilon_m-\varepsilon_f}} \quad \ldots\ldots\ldots\ldots \quad (1)$$

NOMENCLATURE

σ_y^1 true yield stress for softer phase
σ_y^{11} true yield stress for harder phase
f volume fraction of harder phase
E Young's modulus, taken to be 210 GN m^{-2}
v Poisson's ratio, taken to be 0·33
ε_p^1 true plastic strain in softer phase
ε_p^{11} true plastic strain in harder phase
$\varepsilon_p^1(\text{ii})$ critical true plastic strain in soft phase to start yield in hard phase
$\varepsilon_p(\text{ii})$ critical average plastic strain to start yield in hard phase
$\bar{\varepsilon}_p$ true average plastic strain
$Y(\text{i})$ average true stress at the onset of flow in soft phase
$Y(\text{ii})$ average true stress at the onset of flow in hard phase
σ_{33}^A true applied stress
$\delta\varepsilon_p^1$ strain increment in soft phase
$\delta\varepsilon_p^{11}$ corresponding strain increment in hard phase
σ_f^1 true flow stress of soft phase
σ_f^{11} true flow stress of hard phase
A $E(7-5v)/\lvert 10(1-v^2)\rvert$
ε_t total true strain
n strain hardening coefficient
K strengthening coefficient

The subscripts 'm' and 'f' refer to martensite and ferrite, respectively.

where

$$\beta = \frac{\sigma_m \varepsilon_f^{\varepsilon_f} \exp \varepsilon_m}{\sigma_f \varepsilon_m^{\varepsilon_m} \exp \varepsilon_f} \quad \ldots \quad (1a)$$

and σ_m and σ_f are the true tensile strengths of the martensite (or any other hard phase) and ferrite respectively, and ε_c, ε_m, and ε_f are the true uniform strains for the composite, martensite, and ferrite, respectively. The relationship is valid when the true stress/true strain behaviour of the composite and of the component phases can be represented by a power law of the form:

$$\sigma = K\varepsilon^n \quad \ldots \quad (2)$$

where K is the strengthening coefficient.

However, the critical assumptions of this model require, firstly, equal strain distributions in both the hard and the soft phases, and secondly, continuity of the phases in the tensile direction. Hence, the conclusions drawn by the application of Mileiko's theory to dual-phase steels have been criticized recently,[16] especially as it has been shown[16] that different deductions, particularly with respect to strength/formability ratios, can be made by assuming non-uniform strain in the component phases.

Despite the above setbacks, it is apparent that Mileiko's theory does indeed give reasonable agreement with experimental data on the dual-phase steels examined thus far.[13,14] The reasons for this agreement are not clear and it was felt that a more detailed analysis was necessary. The present authors have noted the availability of a more general two-phase deformation theory developed by Tomota *et al.**[17] where the internal stresses produced by inhomogeneous deformation are taken into account. Furthermore, the latter theory applies to the case where the harder (or softer) phase is randomly distributed as grains of ellipsoidal shape (the random distribution ensures an effect approximating spherical grains) and is therefore more representative of dual-phase steel microstructures.

* Henceforth referred to as Tomota's theory for brevity.

Additionally, the stress and strain distributions can be followed at every stage of the deformation process. By this theory, the applied stress before the onset of plastic deformation in the hard phase is given as

$$\sigma_{33}^A = \sigma_f^1 \left| \frac{\bar{\varepsilon}_p}{1-f} \right| + \frac{f}{(1-f)} A\bar{\varepsilon}_p \quad \ldots \quad (3)$$

where

$$\bar{\varepsilon}_p = (1-f)\varepsilon_p^1 \quad \ldots \quad (3a)$$

and the onset of plastic flow in the harder phase is represented by the following set of simultaneous equations:

$$Y(\text{ii}) = \sigma_f^1 \left| \frac{\bar{\varepsilon}_p(\text{ii})}{1-f} \right| + \frac{f}{1-f} A\bar{\varepsilon}_p(\text{ii}) \quad \ldots \quad (4)$$

$$Y(\text{ii}) = \sigma_y^{11} - A\bar{\varepsilon}_p(\text{ii}) \quad \ldots \quad (5)$$

Further deformation is calculated for small strain increments from the following simultaneous equations:

$$\sigma_f^1 \lvert \varepsilon_p^1(\text{ii}) + \delta\varepsilon_p^1 \rvert = \sigma_{33}^A - fA[\varepsilon_p^1(\text{ii}) + (\delta\varepsilon_p^1 - \delta\varepsilon_p^{11})] \quad \ldots \quad (6)$$

$$\sigma_f^{11} \lvert \delta\varepsilon_p^{11} \rvert = \sigma_{33}^A + (1-f)A[\varepsilon_p^1(\text{ii}) + (\delta\varepsilon_p^1 - \delta\varepsilon_p^{11})] \quad \ldots \quad (7)$$

Elastic deformation results in the term (σ_{33}^A/E) being added to the plastic strain of the alloy.

Thus the complete stress/strain curve can be computed and consequently the strain hardening coefficient can also be computed when the curve can be represented by the empirical equation, $\sigma = K\varepsilon^n$. In the analysis that follows, equations of the above form were used to represent the flow stresses of the individual components and of the composite. The strain increment $\delta\varepsilon_p^1$ was taken as 0·01 and it was assumed that the modulus is the same for all the phases. The yield stresses were taken as the true stress at $\varepsilon_t = 0{\cdot}002$.

Mileiko's theory has been successfully applied to analyse the deformation of a zero-carbon ferrite/martensite structure in Fe–3Ni–3Mo,[13] and a ferrite/martensite structure in a vanadium HSLA steel (Fe–0·15C–1·5Mn–0·11V).[14] Considering first the data presented in Ref. 13 for the Fe–3Ni–3Mo alloy, the following deformation parameters can be listed:

$\sigma_y^{11} = 705$ MN m^{-2}
$n_m = 0{\cdot}06$
$n_f = 0{\cdot}24$
$K_m = 1113$ MN m^{-2}
$K_f = 369$ MN m^{-2}

The results of the inhomogeneous deformation analysis by Tomota's method are plotted in Fig. 1 and it is clear that the predictions are essentially the same as those of Mileiko's model. The reason for this becomes apparent from Fig. 2, which shows the plastic strain in the ferrite as a function of that in the martensite, calculated using Tomota's theory. It is clear that the plastic strain difference between the two components is very small, so that the equal strain model is applicable. This agreement with Mileiko's theory arises due to the relatively small amount of plastic strain in the ferrite prior to the onset of plastic flow in the martensite.

Similarly, application of the inhomogeneous deformation model to the data of Ref. 14 for the vanadium HSLA steel showed that the plastic strain difference between the ferrite and martensite components was also sufficiently small to give similar results to those predicted by Mileiko's theory,

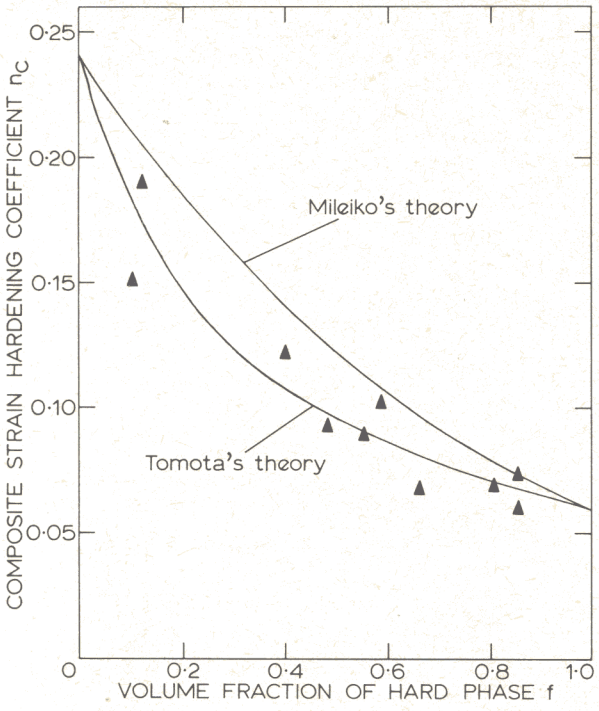

triangular points represent data from Ref. 13

1 Composite strain hardening coefficient vs. volume fraction of hard phase

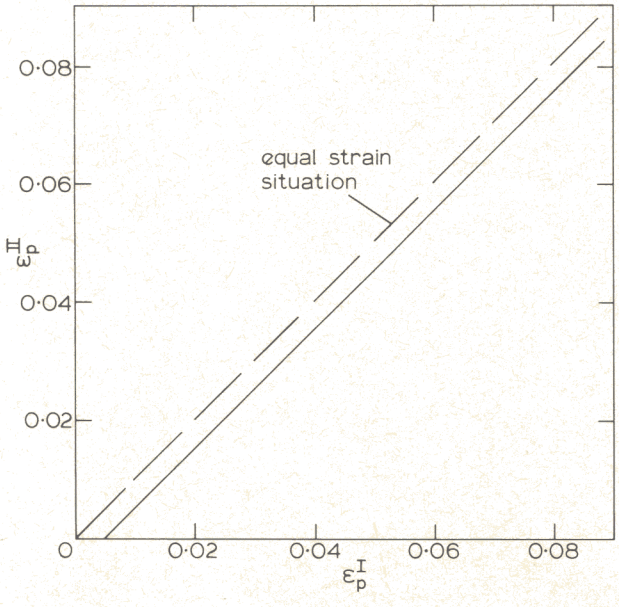

2 Calculated cumulative plastic strain in hard phase ε_p^{II} vs. that in soft phase ε_p^{I}

(Figs 3 and 4). In this analysis the following parameters were used:

$\sigma_y^{11} = 1500$ MN m^{-2}

$n_m = 0{\cdot}08$

$n_f = 0{\cdot}31$

$K_m = 2448$ MN m^{-2}

$K_f = 690$ MN m^{-2}

The values of the strengthening coefficients were calculated

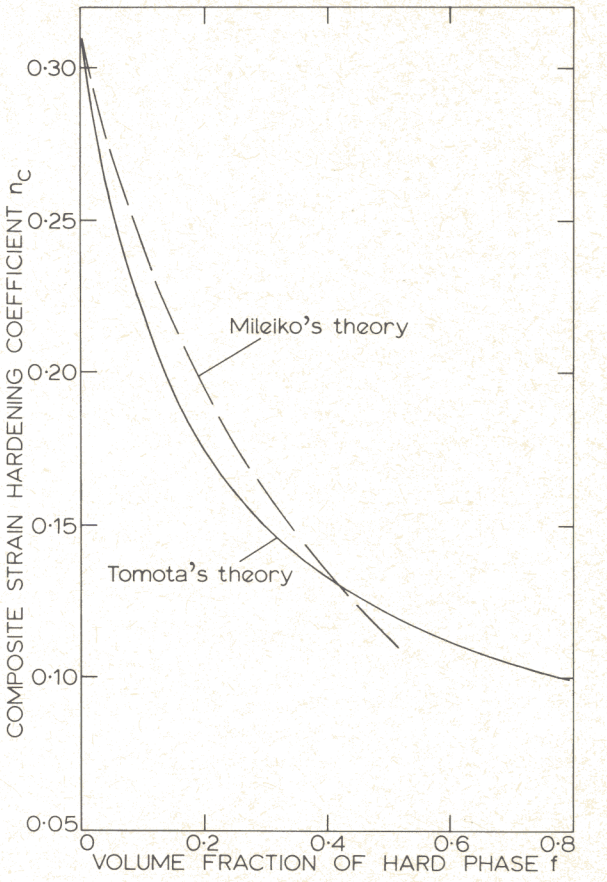

3 Composite strain hardening coefficient vs. volume fraction of hard phase using deformation parameters listed in Ref. 14

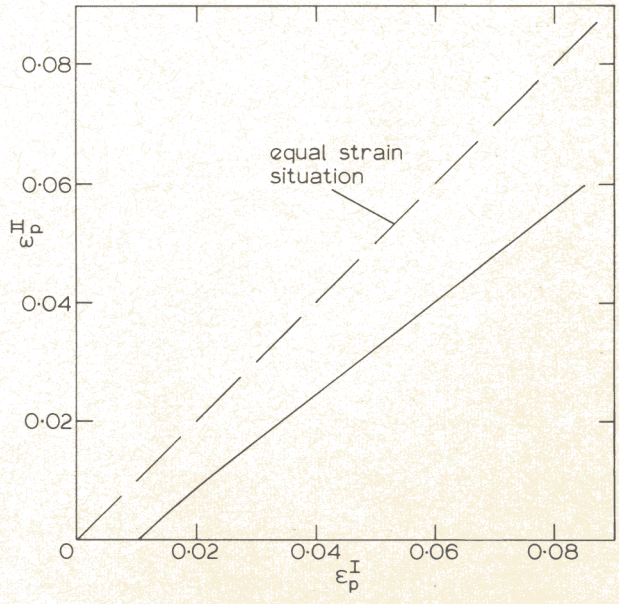

4 Calculated cumulative plastic strain in hard phase ε_p^{II} vs. that in soft phase ε_p^{I}

from the tensile strength values quoted in Ref. 14, assuming that failure was by the ductile mode so that $\sigma_{UTS} = Kn^n$.

EXPERIMENTAL PROCEDURE

A 2 kg melt of the experimental alloy was prepared from pure constituents in a vacuum induction furnace, and the

final analysis was Fe–0·04C–0·63Mn–2·01Si–0·1V. The ingot was hot worked down to 8 mm diameter rod by forging and swaging operations.

During austenitizing heat treatments, the specimens were doubly protected by a dynamic argon atmosphere and a proprietary anti-decarburizing compound. The heat treatments were carried out in a resistance-heated tube furnace.

Tensile specimens were machined from heat-treated blanks with a 50 mm parallel length and a 3 mm diameter. They were tested on an Instron testing machine with a 25 mm gauge length linearly variable differential transformer extensometer. This was attached to the specimen for only a part of the test and the final uniform elongation was measured from 5 mm gauge lengths previously marked on the specimen parallel length, taking care that the measurement was well away from the position of the necked region.

Specimens for transmission electron microscopy were cut from the tensile specimen blanks as 3 mm diameter discs with a thickness of 0·25 mm. The discs were subsequently thinned and electropolished in a twin-jet polishing unit using 25% glycerol, 5% perchloric acid, and 70% ethanol at room temperature and 55 V. The foils were examined in a Philips EM300 microscope at 100 kV.

Quantitative metallography was carried out on a Quantimet image analysing computer.

RESULTS AND DISCUSSION

Microstructural observations

The volume fractions of hard phases obtained by various heat treatments are listed in Table 1. Using these data and the fact that the formation of pro-eutectoid ferrite involves the partitioning of carbon into the residual austenite allowed the carbon content of the hard phase region to be estimated on the assumption that the pro-eutectoid ferrite contained 0·02% carbon in solid solution. The latter assumption is approximate since the exact carbon content of the ferrite will depend on the cooling rate from the transformation temperature. The hardenability of the residual austenite, which is expected to be a sensitive function of its carbon content, will therefore also be a function of the volume fraction of transformation to ferrite. Hence, microstructural differences can be expected with varying ferrite volume fractions. This is particularly true for the present steel where the very low average carbon content imparts poor hardenability.

Air cooling from the austenitizing temperature resulted in a microstructure of pro-eutectoid ferrite and extremely small islands of fine pearlite, the lamellae of which could be resolved by transmission electron microscopy. The volume fraction of the pearlitic phase was about 0·03 (Fig. 5).

Direct quenching into water or iced brine from 1130°C (well above the A_{r3} temperature) gave up to 23% upper bainite. This upper bainite was similar to that observed in higher carbon–silicon-containing steels[10] and consisted of dislocated bainitic ferrite laths separated by discontinuous films of carbon-enriched retained austenite. Additionally, it seemed that the islands of residual austenite transformed into a single crystallographic variant of upper bainite, rather than several variants (partitioning behaviour) as was the more usually observed mechanism in higher carbon steels. The latter observation is probably a manifestation of the fact that the kinetics of bainitic ferrite growth are markedly accelerated by a decrease in carbon content, so that in contrast to the higher carbon–silicon steels, the first variant to nucleate will develop rapidly and consume the whole of the austenite region. Furthermore, the particular variant corresponding to the adjacent pro-eutectoid ferrite will find nucleation relatively easier and will therefore be favoured. This is illustrated in Fig. 6 where the bainitic ferrite plate (arrowed) has the same orientation as the adjacent pro-eutectoid ferrite. The morphology and discontinuous nature of the austenite films is considered elsewhere.[11]

When the quench rate was increased by quenching into agitated iced brine from a higher austenitizing temperature (1300°C), the volume fraction of bainite increased to about 0·33 since there was less time available for the pro-eutectoid ferrite transformation during the quench, Fig. 7.

Quenching from lower austenitizing temperatures (970–920°C) into agitated iced brine resulted in a hard-phase microstructure consisting of platelet martensite separated by films of retained austenite. Autotempering was not evident in the martensite, which was occasionally found to be twinned, Fig. 8.

The ferrite grain size was measured by lineal analysis and the intersections of test lines with the interfaces between hard phase and pro-eutectoid ferrite were included in the determinations. It is seen from Table 1 that the effective ferrite grain size does not vary markedly despite the wide variation in transformation conditions. In view of this, and the fact that uniform elongation is essentially unaffected by ferrite grain size,[5] the latter is not taken into account in the analysis of mechanical properties that follows.

Table 1

Specimen*	Heat treatment			(C)	Volume fraction of hard phase	Effective ferrite grain size, μm
(*a*)	10 min	1130°C	AC	0·62	0·03	23
(*b*)	10 min	1130°C	WQ	0·11	0·22	16
(*c*)	10 min	1130°C	IBQ	0·11	0·23	14
(*d*)	5 min	1300°C	AIBQ	0·08	0·33	18
(*e*)	10 min	920°C	AIBQ	0·25	0·09	30
(*f*)	10 min	970°C	AIBQ	0·16	0·15	24
(g)	10 min	935°C	AIBQ	0·21	0·11	22

* Specimen (*a*) contained pearlite, (*b*), (*c*), and (*d*) contained upper bainite, and (*e*), (*f*), and (g) contained martensite.
AC = air cooled
WQ = water quenched
IBQ = iced brine quench
AIBQ = agitated iced brine quench
(C) = carbon content of the hard phase region assuming that the carbon level in the pro-eutectoid ferrite is 0·02 wt-%.

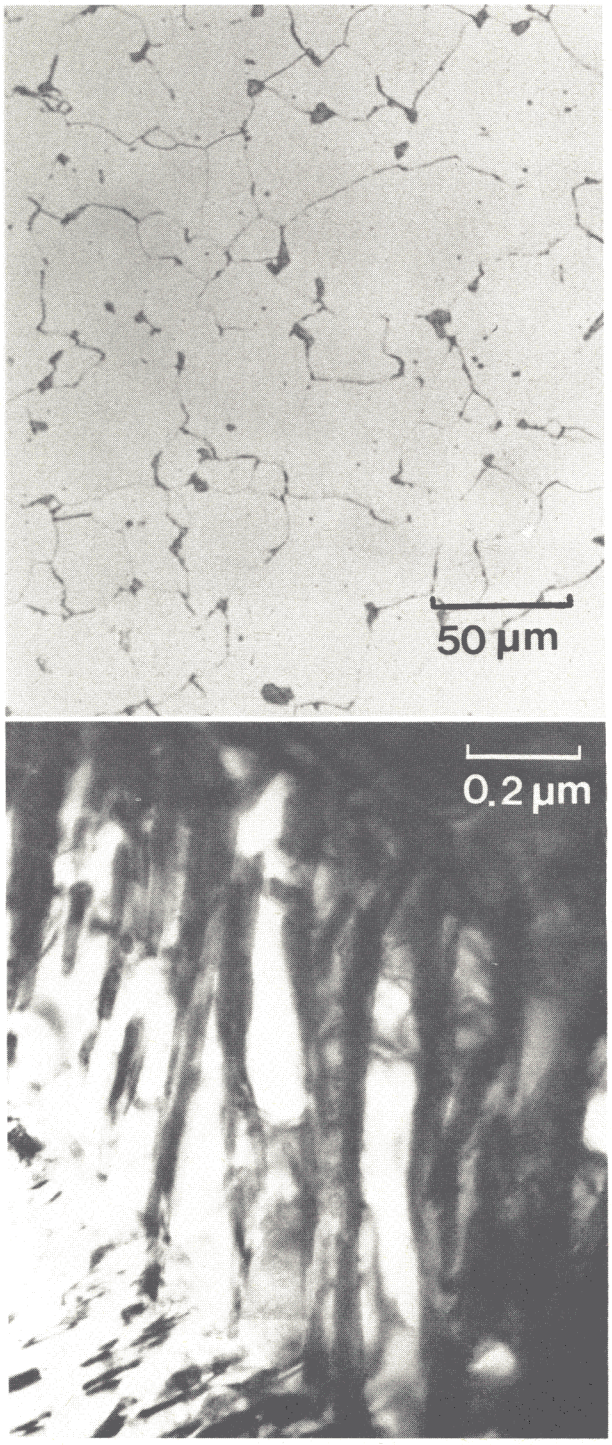

a optical micrograph; *b* bright field image of island of pearlite

5 Samples air cooled following austenitization at 1130°C for 10 min

Mechanical properties

The deformation parameters obtained are listed in Table 2. The true stress/true strain curves were found to be accurately represented by equation (2). These curves are plotted in Fig. 9 and the variation of the strain hardening and strengthening coefficients as a function of the volume fraction of hard phase is plotted in Fig. 10. In the case of the air-cooled specimen, the use of equation (2) is approximate and leads to an under estimation of flow stress at high strains. However, the disagreement is sufficiently small for the purposes of the following calculations. The data from the air-cooled specimen were taken to be approximately representative of the deformation characteristics of pure ferrite in the present steel since it contained only 3% pearlite.

The first stage of deformation was analysed in terms of equation (1) when it was assumed that at $\varepsilon = 0{\cdot}002$, there was zero plastic strain in the hard phase, Fig. 11*a*. This assumption is necessary due to the absence of data for this alloy in the pure bainitic or martensitic states; 100% transformation to these microstructures was impossible due to the low hardenability of the alloy used. By systematically varying σ_y^{11}, n_2, K_2, it proved possible to estimate the most likely values of these parameters by noting the set which gave the best fit with the experimental composite stress/strain parameters. Thus, the following values were deduced:

Bainite	*Martensite*
$\sigma_y^{11} = 1000$ MN m^{-2}	$\sigma_y^{11} = 1300$ MN m^{-2}
$K_2 = 5200$ MN m^{-2}	$K_2 = 6500$ MN m^{-2}
$n_2 = 0{\cdot}300$	$n_2 = 0{\cdot}327$

The above values are considered to be realistic for the high-silicon microstructures, and compare well with the values obtained for an Fe–0·3C–3Cu–1Si alloy isothermally transformed at 510°C to give a microstructure of silicon upper bainite and some martensite.[11] The strain hardening coefficient in the latter microstructure was found to be 0·48, the strengthening coefficient was 3130 MN m^{-2}, and the yield stress was 980 MN m^{-2}.

Comparison of the experimental data with the values predicted by Tomota's theory using the above parameters, is illustrated in Fig. 11. Using the above deformation parameters, Mileiko's theory was found to overestimate considerably the composite strain hardening coefficients (at $f = 0{\cdot}1$, $n_c = 0{\cdot}21$, and at $f = 0{\cdot}2$, $n_c = 0{\cdot}23$). The reason for this can be understood from Fig. 12, which shows the variation of plastic strain in the two components. In the present steel, the deformation characteristics of the bainite and martensite on the one hand, and ferrite on the other, are sufficiently different to give extremely inhomogeneous strain distribution. Thus much of the deformation is concentrated in the ferrite. Since the intrinsic strain hardening coefficient of the latter is low, the general composite strain hardening coefficient will be lower than predicted by an equal strain deformation model. The requirements of Mileiko's theory are clearly not justified with the present steel and agreement is poor. Tomota's theory, however, gives good agreement with the experimental data and reflects the more general applicability of the model to dual-phase steels. (It should be noted that while the failure to obtain 100% hard phase microstructures in the present experimental steel prevented the full predictive use of Tomota's theory, the predicted best fitting deformation parameters for the hard phases concerned are realistic.)

From Table 2 it is noted that the uniform elongation (as determined by measurements made on the gauge length well away from the necked region) does not in fact correspond to the magnitude of the strain hardening coefficient but shows a negative correlation. This is attributed to the fact that the hard phases concerned fail prematurely in a non-ductile manner due to rapid strain hardening.

SUMMARY

The applicability of Mileiko's theory to dual-phase steels has been compared with that of a more general two-phase deformation model due to Tomota *et al.* Published data on

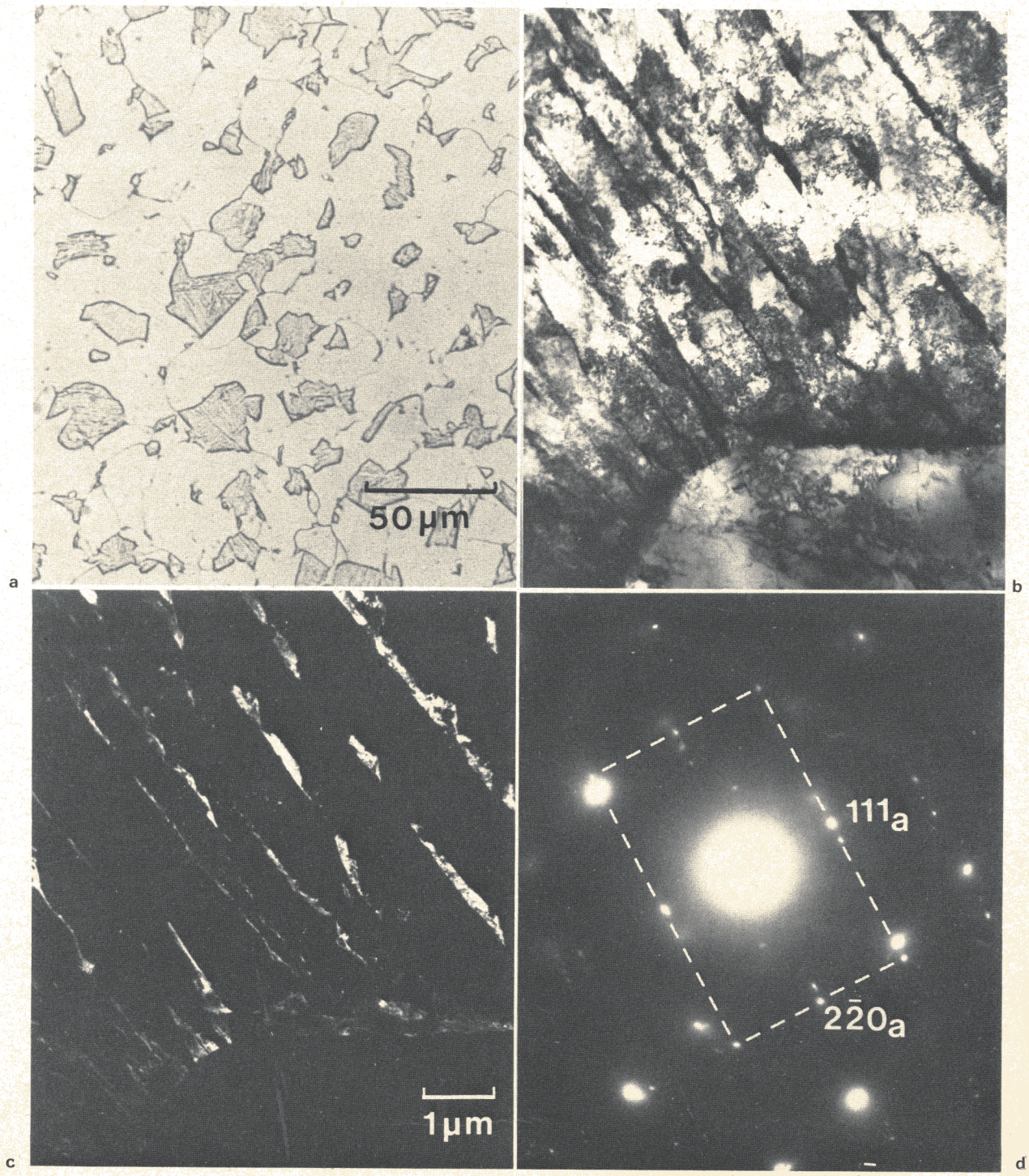

a optical micrograph; *b* bright field image; *c* retained austenite dark field image; *d* corresponding diffraction pattern

6 Sample water quenched following austenitization at 1130°C for 10 min

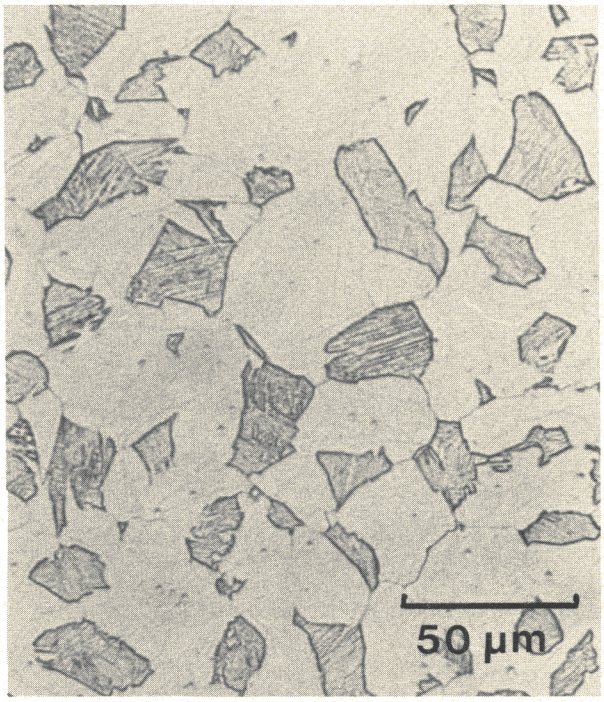

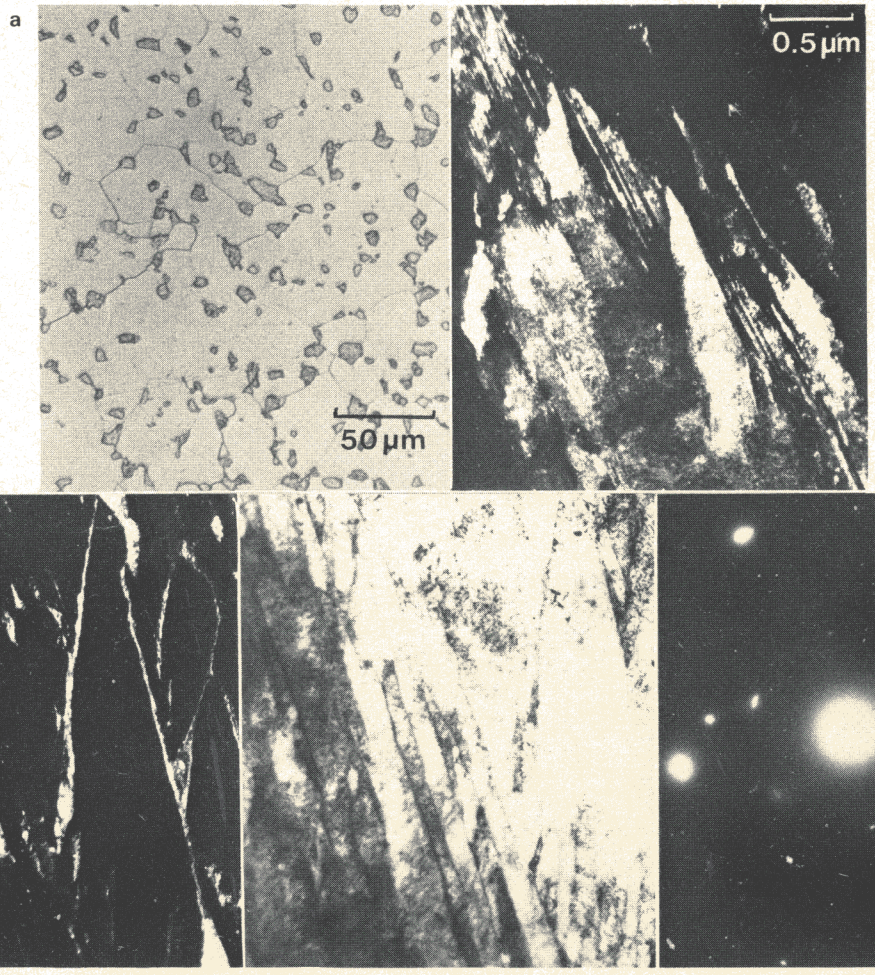

a optical micrograph; *b* dark field image of twins in martensite; *c* dark field image of retained austenite in another island of martensite; *d* corresponding bright field image; *e* corresponding diffraction pattern

8 Sample austenitized at 935°C for 10 min and quenched into agitated iced brine

Table 2 Mechanical properties

Specimen	n	K/MN m^{-2}	UTS/MN m^{-2}	True uniform elongation	True stress at $\varepsilon = 0{\cdot}002$/MN m^{-2}
(*a*)	0·066	504	529	0·153	337
(*b*)	0·144	956	657	0·119	385
(*c*)	0·153	1042	674	0·106	397
(*d*)	0·174	1322	738	0·075	435
(*e*)	0·132	839	629	0·142	372
(*f*)	0·165	1041	659	0·102	368
(*g*)	0·156	1005	656	0·102	383

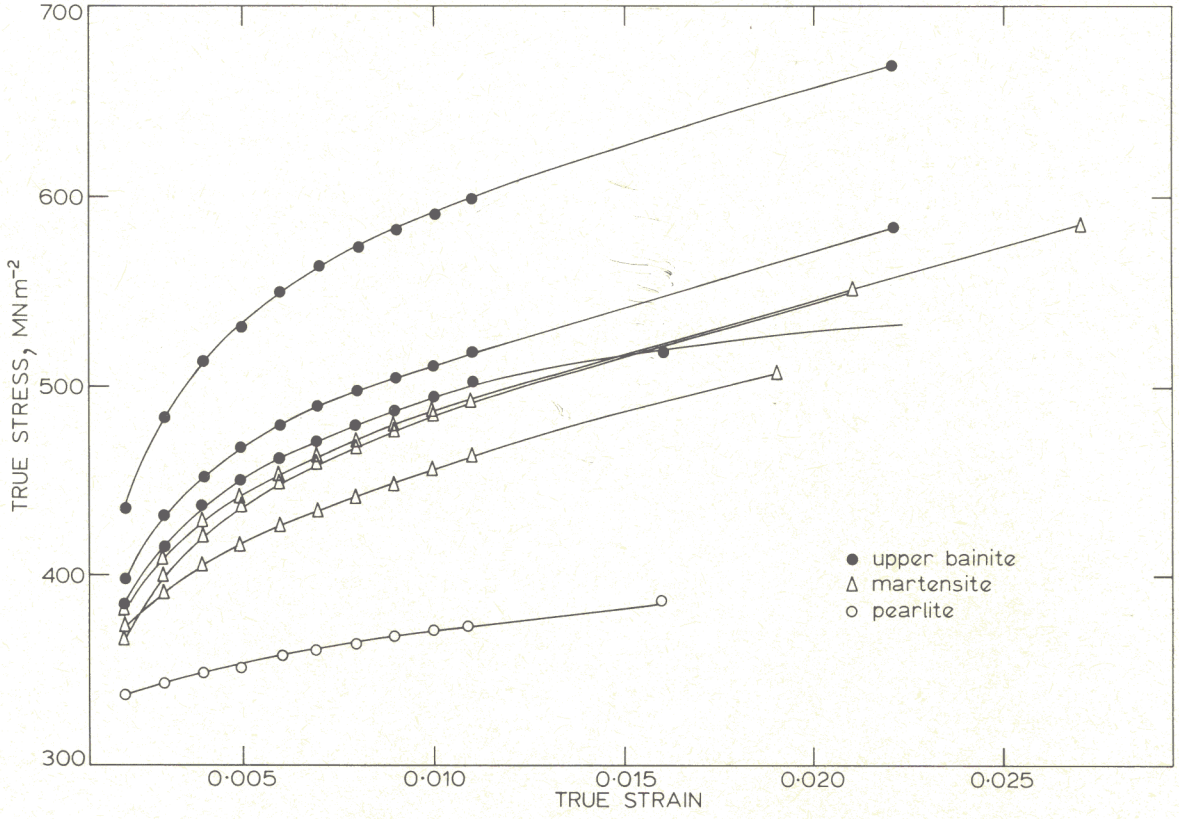

9 True stress vs. true strain curves for various microstructures examined

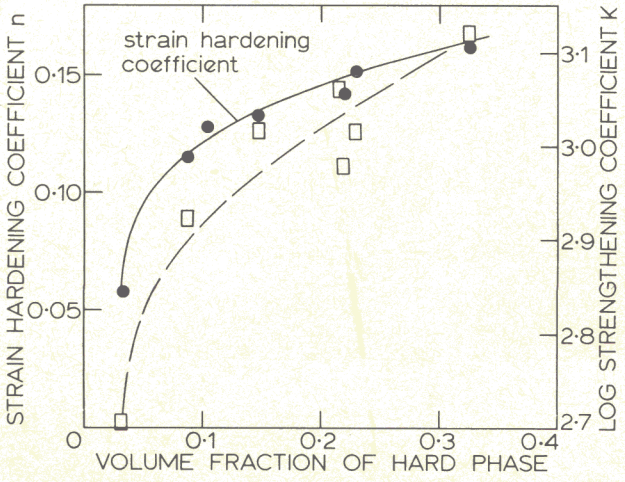

10 Variation of strengthening and strain hardening coefficients as functions of volume fraction of hard phase

dual-phase steels were found to be consistent with the latter model, with the predicted behaviour also being very similar to that found using Mileiko's theory. The apparently good agreement between the experimental results and the predictions using Mileiko's theory was shown to be due to the approximately homogeneous strain distribution (a necessary assumption of Mileiko's model) in the hard and soft phases of the steels whose data were analysed. The greater applicability of Tomota's theory is clear, not only from its less restrictive assumptions as far as dual-phase steels are concerned, but because by using an experimental steel it was demonstrated that Tomota's theory could be equally applied to situations of inhomogeneous strain distribution whereas that of Mileiko expectedly gave poor agreement.

The microstructure of the hard phases obtainable in the experimental high-silicon dual-phase steel used for the above analysis were also characterized in detail by transmission electron microscopy. Depending on the heat-treatment condition the hard phase acicular structures were identified either as martensitic plates separated by thin films of retained austenite, or as carbide-free upper bainitic ferrite plates, also associated with carbide-free retained austenite.

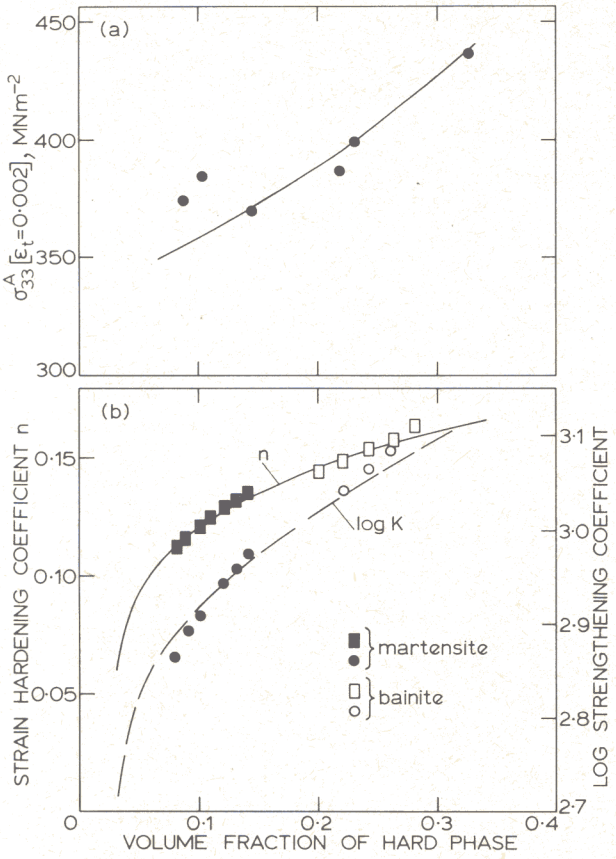

lines represent experimental curves from Fig. 10

11 *a* σ_{33}^{A} **vs. volume fraction of hard phase;** *b* **best fit calculated values of strengthening and strain hardening coefficients obtained using Tomota's theory vs. volume fraction of hard phase**

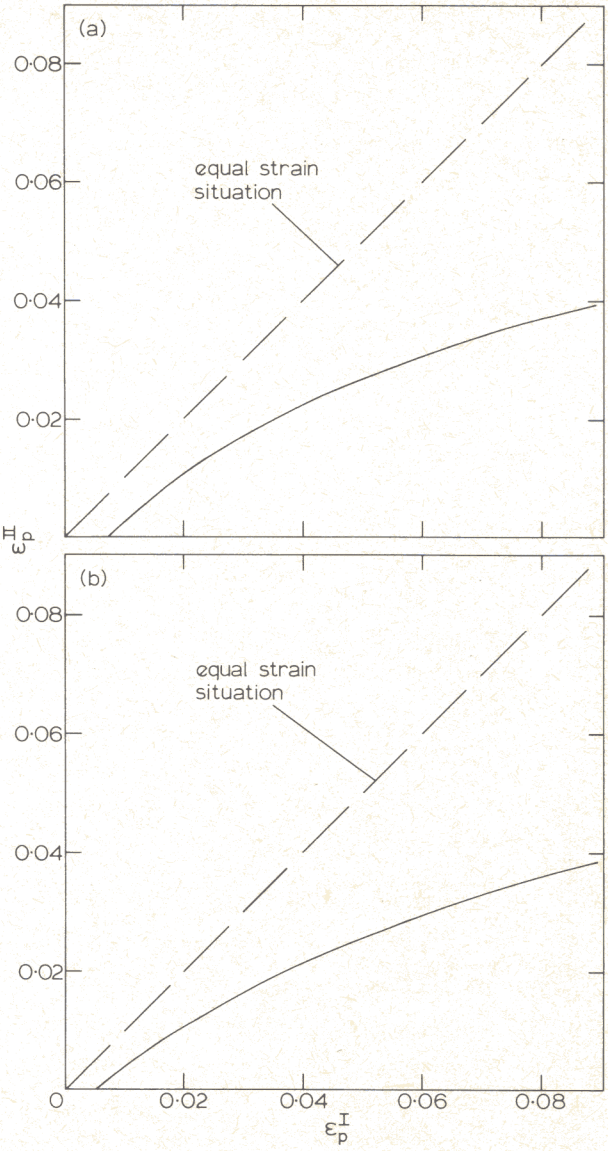

a hard phase of martensite; *b* hard phase of bainite

12 Calculated cumulative plastic strain in hard phase ε_p^{II} vs. that in soft phase ε_p^{I}

ACKNOWLEDGMENTS

The authors are grateful to Professor R. W. K. Honeycombe for the provision of laboratory facilities and for his encouragement during the course of this work, and to the Ministry of Defence (RARDE), Fort Halstead, for their financial support. DVE also wishes to thank the Royal Society for the Warren Research Fellowship.

REFERENCES

1. M. S. RASHID: SAE preprint 760206, February 1976.
2. M. S. RASHID: SAE preprint 770211, February 1977.
3. P. E. REPAS: Seminar on 'Vanadium cold pressing and dual-phase steels', VANITEC, West Berlin, 1978, paper no. 2.
4. R. G. DAVIES and C. L. MAGEE: Ref. 3., paper no. 3.
5. R. G. DAVIES: *Metall. Trans. A*, 1979, **10,** 113.
6. R. G. DAVIES: 'On the ductility of dual-phase steels', Dearborn, Michigan, Ford Motor Co.
7. W. S. OWEN: *Trans. ASM*, 1954, **46,** 812.
8. J. GORDINE and I. CODD: *J. Iron Steel Inst.*, 1969, **207,** 461.
9. R. M. HOBBS, G. W. LORIMER, and N. RIDLEY: *ibid.*, 1972, **210,** 757.
10. H. K. D. H. BHADESHIA and D. V. EDMONDS: *Metall. Trans. A*, 1979, **10,** 895.
11. H. K. D. H. BHADESHIA and D. V. EDMONDS: unpublished research.
12. R. F. HEHEMANN: 'Phase transformations', 397, 1970, Metals Park, Ohio, ASM.
13. R. G. DAVIES: *Metall. Trans. A*, 1978, **9,** 451.
14. R. G. DAVIES: *ibid.*, 1978, **9,** 41.
15. S. T. MILEIKO: *J. Mater. Sci.*, 1969, **4,** 974.
16. R. LAGNEBORG: Seminar on 'Vanadium cold pressing and dual-phase steels', VANITEC, West Berlin, 1978, paper no. 5.
17. Y. TOMOTA, K. KUROKI, T. MORI, and I. TAMURA: *Mater. Sci. Eng.*, 1976, **24,** 85.

Same f, but different c
Bruschinger
Effect of Si
Effect of grain size